



HAL
open science

Use of spherical indentation data changes to materials characterization based on a new multiple cyclic loading protocol

Jean-Marc Collin, Gérard Mauvoisin, Philippe Pilvin, Rochdi El Abdi

► **To cite this version:**

Jean-Marc Collin, Gérard Mauvoisin, Philippe Pilvin, Rochdi El Abdi. Use of spherical indentation data changes to materials characterization based on a new multiple cyclic loading protocol. *Materials Science and Engineering: A*, 2008, 488, pp.602-622. 10.1016/j.msea.2008.01.041 . hal-01007414

HAL Id: hal-01007414

<https://hal.science/hal-01007414>

Submitted on 15 Dec 2018

HAL is a multi-disciplinary open access archive for the deposit and dissemination of scientific research documents, whether they are published or not. The documents may come from teaching and research institutions in France or abroad, or from public or private research centers.

L'archive ouverte pluridisciplinaire **HAL**, est destinée au dépôt et à la diffusion de documents scientifiques de niveau recherche, publiés ou non, émanant des établissements d'enseignement et de recherche français ou étrangers, des laboratoires publics ou privés.

Use of spherical indentation data changes to materials characterization based on a new multiple cyclic loading protocol

Jean-Marc Collin^{a,*}, Gérard Mauvoisin^a, Philippe Pilvin^b, Rochdi El Abdi^a

^a LA.R.M.A.U.R., FRE CNRS 2717, Campus de Beaulieu, Université de Rennes 1, 35042 Rennes Cedex, France

^b L.G.2M., Université de Bretagne-Sud, Rue de Saint-Maudé, BP 92116, 56321 Lorient Cedex, France

An interpretation of spherical indentation experiments and the determination of hardening law parameters is the challenge in this paper. A new protocol based on multiple cyclic loading allowed models describing the indentation data changes to be determined from a numerical study. Inversion of these models, determined for two constitutive equations with isotropic hardening, combined with a sensitivity study enabled the study of the uniqueness of the solution. It is shown that although the new protocol is not necessary to determine the two Hollomon equation parameters, it is necessary to determine accurate values of the three Ludwik equation parameters.

From an experimental study, it was shown that methods based on a “reverse” analysis can be used in order to have an evaluation of the mechanical properties in a first-order approximation.

Keywords: Spherical indentation; Materials characterization; Multiple cyclic loading

1. Introduction

An instrumented indentation test consists in measuring, simultaneously, the indentation load P and the indentation depth h during the penetration of an indenter into a sample. This test can be used in order to determine some parameters of the work-hardening behavior law of the tested sample. The more commonly used is the Hollomon isotropic work-hardening law defined by the following equation:

$$\sigma = \sigma_y^{1-n} E^n \varepsilon^n \quad (1)$$

This relationship gives, in the case of a monotonic sollicitation in the elasto-plastic regime, the material flow stress. E , σ_y , n and ε , are, respectively the Young modulus, the yield stress, the work-hardening exponent and the strain.

The first identified parameter, from an indentation test, is the reduced Young modulus E^* defined by $E^* = [(1 - \nu_i^2)/E_i + (1 - \nu_s^2)/E_s]^{-1}$, where ν is the Poisson ratio, s stands for “sample,” whereas i stands for “indenter”. The determination of E^* is based on the Hertz elastic contacts theory [1].

Sneddon [2] proposed a general solution to the problem of an elastic sample indented by any shape of indenter. In the case of spherical indentation, the contact stiffness is defined as follows:

$$S = \frac{dF}{dh} = 2E^* a \quad (2)$$

where a is the contact radius. When the elastic regime is over, Eq. (2) can still be applied at the beginning of the unloading [3–5]. Following this, Doerner and Nix [6], Loubet et al. [7] and Oliver and Pharr [8] proposed to deduce E^* from an indentation test using relationship (2). These methods can be distinguished from one another by the way the contact radius is evaluated. Lastly, Hay and Wolff [9] proposed a correction for the application of the Hertz theory by introducing a factor in order to take into account the radial displacements of material under the indenter.

Concerning the non-elastic behavior, many methods have been proposed to deduce the mechanical parameters, usually deduced from a tensile test, from an indentation test. These methods can be distinguished from one another by the indenter they use (Vickers, sharp, spherical, etc.) and the data they use. Moreover, two kinds of methods can be used to extract mechanical properties from the indentation test. The first is based on the inversion of models established from a numerical study and is called a “reverse” analysis. The second is based on an “inverse”

* Corresponding author. Tel.: +33 2 2323 6282.

E-mail address: jean_marc.collin@yahoo.fr (J.-M. Collin).

analysis. The greater part of established methods are based on a “reverse” analysis, however, Nakamura et al. [10] proposed the determination of the properties of graded materials by using an “inverse” analysis protocol in spherical indentation. We can also quote Bolzon et al. [11] who applied “inverse” analysis to conical indentation. Most of the “reverse” analysis methods are based on the modelling of the representative strain introduced by Tabor [12]. Dao et al. [13] proposed to extract the Eq. (1) parameters from a unique sharp indentation. They also showed that the determined parameters are very sensitive to small variations in the indentation data. This work has been followed by Chollacoop et al. [14] who applied the previous method with two sharp indenters with different apex angles. Then, they showed an improvement in the determination of the material properties with two indenters. Moreover, the use of two sharp indenters significantly decreased the sensitivity of the predicted parameters to the perturbations in the indentation data. Bucaille et al. [15] also proposed using different sharp indenters in order to solve the problem.

The uniqueness of the solution has been fully studied by Cheng and Cheng [16], who demonstrated that in the case of sharp indentation, several sets of Eq. (1) parameters can lead to the same $P(h)$ curve. However, they demonstrated that this problem does not occur in spherical indentation. Indeed, the method of Dao et al. [13] has been extended to the spherical indentation by Cao and Lu [17] and led to a unique determination of the Eq. (1) parameters. We can also quote Beghini et al. [18] who determined Eq. (1) parameters from the inversion of a $P(h)$ curve model in spherical indentation.

This paper deals with a study of the uniqueness of the solution in the case of spherical indentation. Moreover, we propose an experimental method based on a “reverse” analysis to evaluate the parameters of two constitutive equations by using a unique indenter and a new multiple cyclic loading protocol.

2. Data deduced from an indentation test

Depending on the kind of loading, different data can be deduced from an indentation test (see Fig. 1, the curves of which are deduced from numerical results). If the test consists of a unique loading, the $P(h)$ curve and the total energy $W_t(h)$ changes can be deduced. If the test consists of a loading and an unloading cycle, in addition to $P(h)$ and $W_t(h)$, both the elastic $W_e(h_{max})$ and plastic $W_p(h_{max})$ energies at the end of the loading can be deduced. Moreover, we can deduce the contact stiffness $S(h_{max})$ (defined in Eq. (2)) at the maximal load. Finally, if the test consists of n loading, unloading and reloading cycles, in addition to the previous data we can deduce n points of $W_e(h_{(max)i})$, $W_p(h_{(max)i})$ and $S(h_{(max)i})$ changes. Moreover, from the energies, we can deduce the energy ratio changes as $W_p/W_t(h_{(max)i})$, $W_e/W_t(h_{(max)i})$ and $W_e/W_p(h_{(max)i})$.

Among the three energies, only two are independent. Indeed, they are linked by

$$W_p = W_t - W_e \quad (3)$$

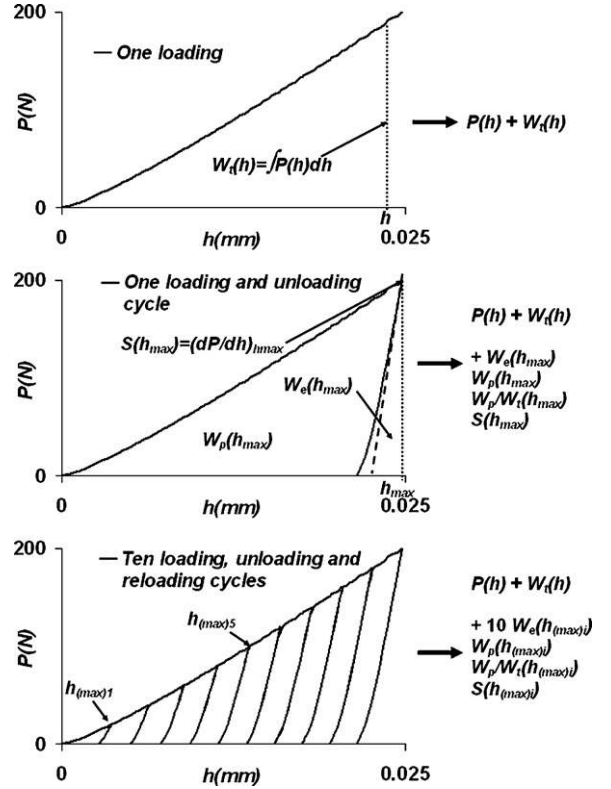


Fig. 1. Different kinds of loading cycles lead to different indentation data.

Moreover, only one energy ratio is sufficient in order to deduce the two others. Indeed, they are linked by

$$\frac{W_p}{W_t} = 1 - \frac{W_e}{W_t} = \left(1 + \frac{W_e}{W_p}\right)^{-1} \quad (4)$$

This is the reason why, for the three energies, we propose to study both the elastic and total energies. Moreover, although the W_p/W_t ratio is linked to the two studied energies, we propose to study it in order to limit the errors of modelling. Concerning the contact stiffness S , because it is obtained by derivating the $P(h)$ curve, it is very sensitive to oscillations of the $P(h)$ curve. For this reason this data is not studied in the following numerical study. Thus, this study concerns the $P(h)$, W_e , W_t and W_p/W_t changes during a spherical indentation test which are deduced from 10 loading, unloading and reloading cycles.

3. Numerical study

3.1. Presentation

A numerical study was conducted in axi-symmetric mode with the finite element (FE) code Cast3M. Fig. 2 shows the FE model where the axi-symmetric boundary conditions are imposed on the axi-symmetric axis.

The sample is modelled by a bulk divided into several areas. In the contact area, the mesh is made of 8-node elements (named QUA8 in the FE code) with quadratic interpolation. In this area, the size of the elements is less than $4 \mu\text{m}$ in order to obtain $P(h)$ curves with the lowest oscillations. The rest of the sample is

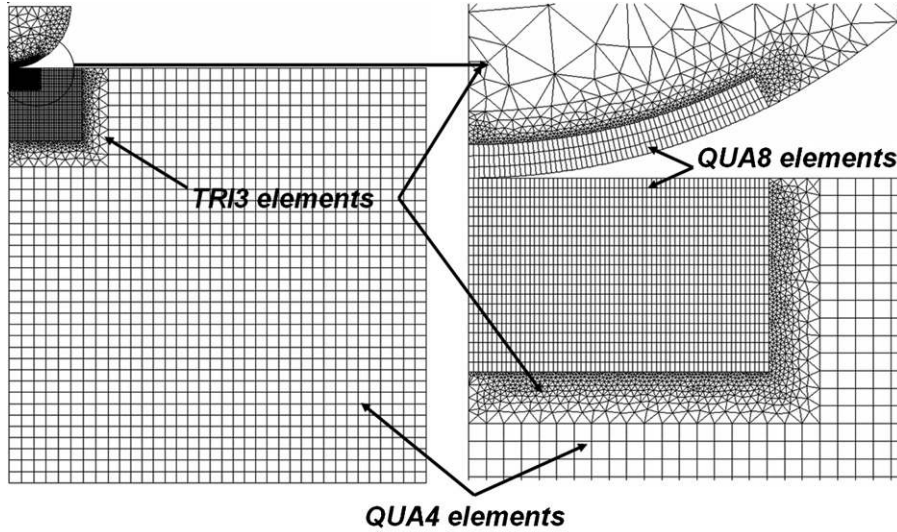


Fig. 2. The FE mesh.

modelled by two areas composed of 4-node elements (named QUA4 in the FE code) with linear interpolation. In the first area, the size of elements is multiplied by 4 and by 80 in the second. Areas with 8-node elements or 4-node elements are separated with transition areas composed of 3-node elements (named TRI3 in the FE code) with linear interpolation.

Concerning the indenter, it is modelled by a quarter of a sphere divided into two areas. In the contact area, as for the sample, the mesh is made of 8-node elements with quadratic interpolation. The rest of the indenter is modelled by an area composed of 3-node elements with linear interpolation.

Because the contact is made between the superior line of the sample and the inferior line of the indenter, the middle nodes of the QUA8 elements are free. In order to solve this problem, two new lines have been created. They are composed of segment elements with linear interpolation. For n QUA8 elements, we have $2n - 1$ nodes in these new lines. Although the friction influence is not negligible, the contact is made without friction between the two new lines in order to focus the study to the plasticity phenomenon.

The sample is described by elasto-plastic behavior with isotropic work hardening. Two constitutive equations have been studied, the Hollomon one (Eq. (1)), and the Ludwig one (Eq. (5)):

$$\sigma = \sigma_y + K\varepsilon^m \quad (5)$$

where K and m describe the work-hardening behavior. It is important to note that Eq. (1) depends on the total strain whereas Eq. (5) depends on the plastic strain only. In this study, the sample's Young modulus is $E_s = 210$ GPa and the Poisson ratio $\nu_s = 0.3$ (which corresponds to that of steel).

The indenter is described by an elastic behavior with $E_i = 600$ GPa and $\nu_i = 0.3$ (which corresponds to a tungsten carbide). The indenter radius is fixed to $R = 0.5$ mm.

In order to follow indentation data changes, 10 loading, unloading and reloading cycles with a maximal load equal to $P_{\max} = 200$ N have been programmed. All the nodes of the superior line of the indenter have the same displacement and the load is applied on the first left node of this line. The indenter

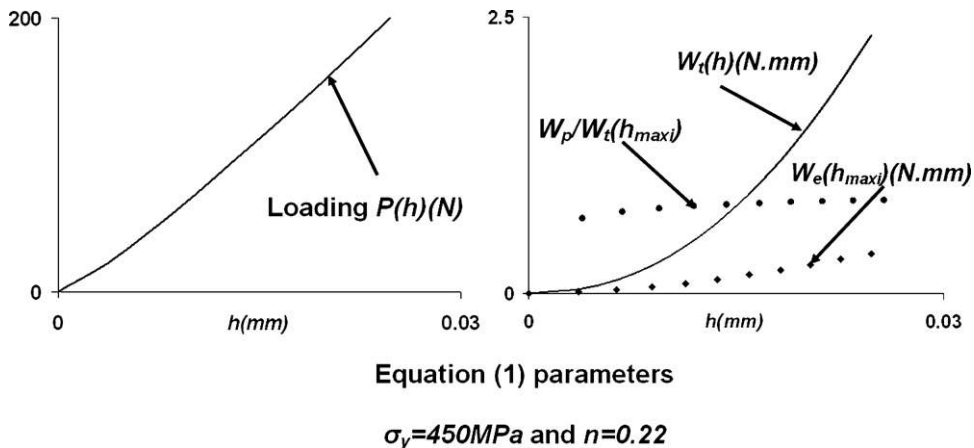


Fig. 3. Typical data deduced from the numerical simulations.

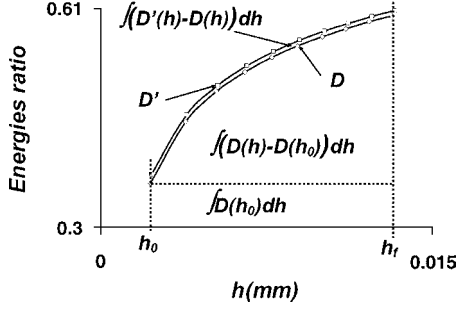


Fig. 4. Quantification of the sensitivity.

moves down into the sample with the bottom of the sample fixed. Figs. 1 and 3 present the typical $P(h)$ curve obtained from the numerical study from which the loading $P(h)$ curve, W_e , W_t and W_p/W_t changes are deduced.

3.2. Sensitivity study

The aim of this paragraph is to study the influence of a variation of each behavior law parameter to the indentation data. We can write the sample's behavior law as a function f (Eq. (6)) of nx_i behavior law parameters and the strain ε :

$$\sigma = f(x_1, \dots, x_i, \dots, x_n, \varepsilon) \quad (6)$$

Thus, indentation data D can be written as a function g (Eq. (7)) of the nx_i behavior law parameters and the indentation depth h :

$$D = g(x_1, \dots, x_i, \dots, x_n, h) \quad (7)$$

If we apply a variation to one parameter x_i which becomes x'_i , the indentation data becomes D' and can be written as follows:

$$D' = g(x_1, \dots, x_i, \dots, x_n, h) \quad (8)$$

We propose to quantify the sensitivity of indentation data D to the parameter x_i (noted $S(D/x_i)$) with the following function:

$$S(D/x_i) = \frac{\int_{h_0}^{h_f} (D'(h) - D(h)) dh}{\int_{h_0}^{h_f} (D(h) - D(h_0)) dh} \quad (9)$$

where h_0 and h_f are presented in Fig. 4. Function (9) has been chosen in order to have an average sensitivity

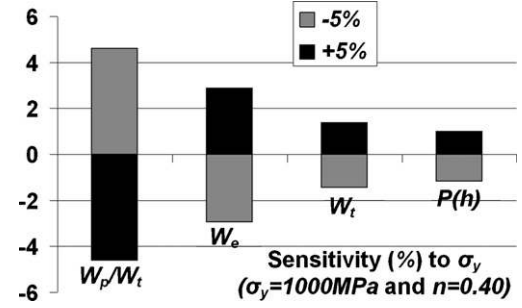


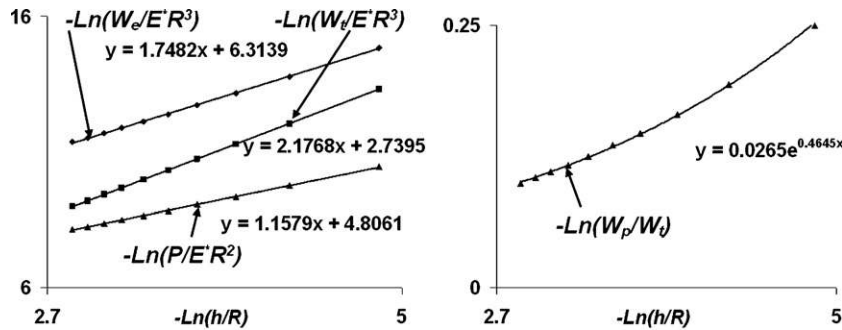
Fig. 5. Symmetry between +5% and -5% on the sensitivity.

which takes into account the initial value of the indentation data.

In the present work, we have studied the sensitivity of the indentation data to Eq. (5) parameters, i.e. the yield stress σ_y and the two work-hardening parameters K and m . However, in order to make a graphic representation of the sensitivity changes possible, we distinguish the sample behavior into a yield stress part and a work-hardening part, we then use Eq. (1) notations. Thus, work hardening is represented by the coefficient n of the Eq. (1). In other words, the evolution of the sensitivity of indentation data to σ_y , K or m will be presented as a surface which depends on the yield stress and the work hardening quantified by n . Twelve sets of parameters have been chosen in order to study the evolution of the sensitivity from a low to a high yield stress ($\sigma_y = 150$ MPa to $\sigma_y = 1000$ MPa) and from a low to high work hardening (quantified by $n=0.02$ to $n=0.4$).

For each set of parameters, we have determined σ_y , K and m which minimize the difference between Eqs. (5) and (1) in order to have the same flow stress curve. For example, a Hollomon sample with $\sigma_y = 150$ MPa and $n = 0.02$ corresponds to a Ludwig sample with $\sigma_y = 150$ MPa, $K = 24.53$ MPa and $m = 0.203$. The indentation behavior of these 12 samples has been simulated, and the data deduced from these simulations are considered as the initial ones (D in Eq. (7)).

In order to verify the symmetry of the sensitivity, a variation of +5% and -5% has been applied on σ_y , K and m for each sample (which leads to 72 simulations). We deduced from these simulations the D' data (in Eq. (8)) for a variation +5% and



Equation (1) parameters :
 $\sigma_y=450$ MPa and $n=0.15$

Fig. 6. Determination of the functions which describe the indentation data changes.

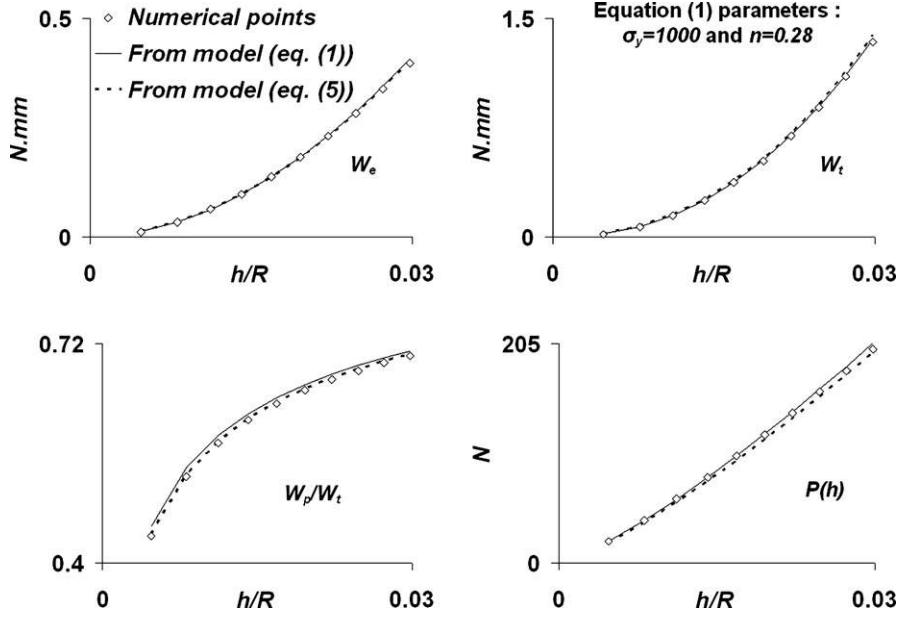


Fig. 7. Comparison between numerical curves and prediction of the models.

−5% of the Eq. (5) parameters. We can observe in Fig. 5 that the sensitivity is symmetric data. Thus, we will consider the sensitivity as the average of the absolute values of the sensitivity to +5% and −5%.

The results of the sensitivity study are presented in Fig. A1 (Appendix A). This is composed of four lines representing the sensitivity of the four indentation data W_e , W_t , W_p/W_t and $P(h)$, respectively. The three columns present the sensitivity to the three parameters σ_y , K and m . For example the first graph in the left top corner shows the sensitivity of the W_e changes to the yield stress in function of the yield stress and the work hardening (quantified by n). In the following presentation, we discuss the global trend of the sensitivity changes to the yield stress and to the work-hardening parameters.

Concerning the evolution of the sensitivity to the yield stress (first column), W_e , W_t and $P(h)$ present the same trend. Moreover, the sensitivities of W_t and $P(h)$ are quite similar. It can be explained by the relationship (10) between W_t and $P(h)$:

$$W_t = \int_{h_0}^{h_f} P(h)dh \quad (10)$$

The most important result of the study of the sensitivity to the yield stress is that it increases when the work hardening decreases. We can observe that the work hardening (quantified by n) has a more important influence than the yield stress on the sensitivity changes except for W_p/W_t .

Concerning the evolution of the sensitivity to the work-hardening coefficients (second and third columns), we can

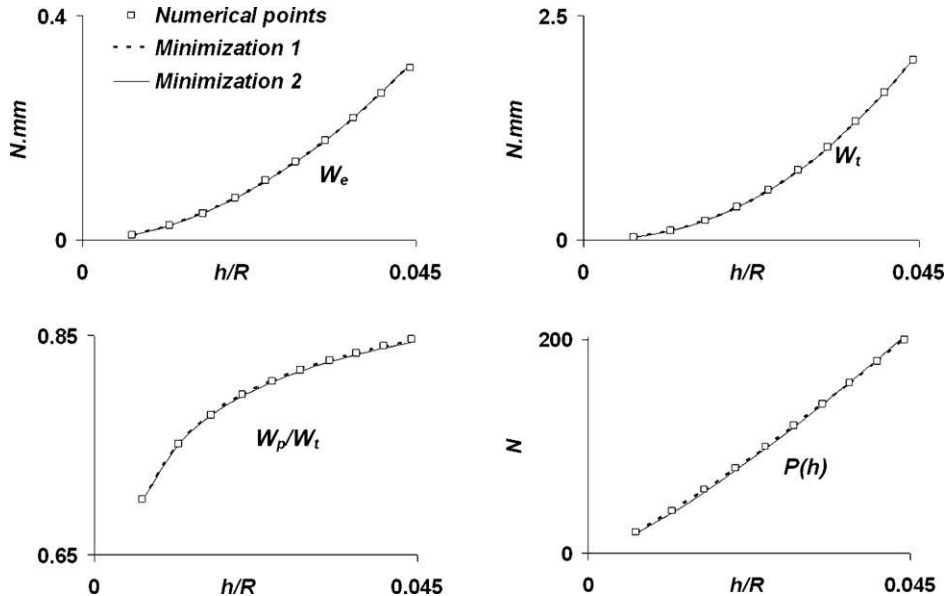


Fig. 8. Several sets of Eq. (5) can lead to the same curve.

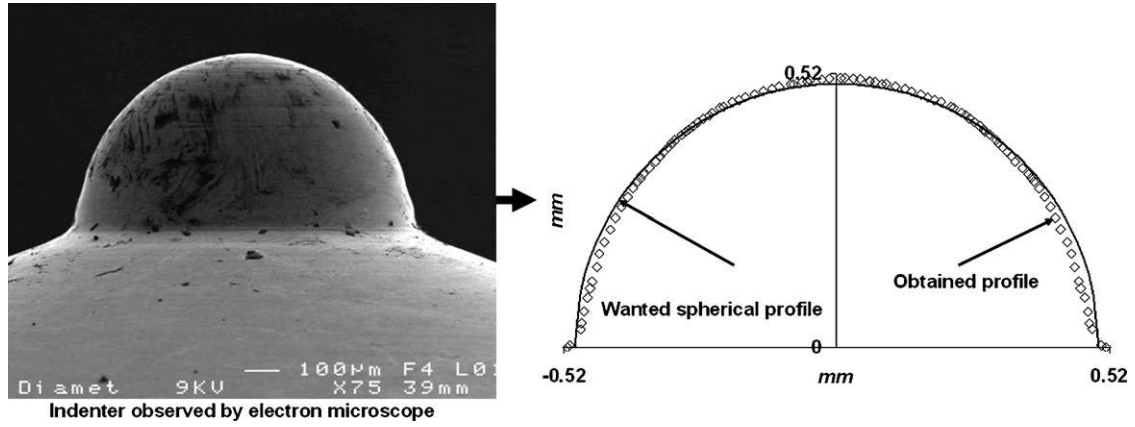


Fig. 9. Our indenter and its profile.

observe that the sensitivity to K and m have the same trend. However, the sensitivity to m is higher than the sensitivity to K . The most important result of the study of the sensitivity to the work-hardening coefficients is that no indentation data is sensitive to the work hardening when this work hardening is very low.

We can conclude that the sensitivity can be divided into sensitivity to the yield stress and sensitivity to the work hardening. The maximum value of the sensitivity to the yield stress is compensated by the minimum value of the sensitivity to the work hardening. Moreover, from this study, W_e seems to be the most sensitive data.

3.3. Determination of models for the four studied indentation data

The area of the materials studied in the previous paragraph has been extended by considering the large domain of σ_y/E_s , in order to cover a large area of metallic materials. The yield stress

varies between 150 and 3000 MPa (150, 450, 720, 1000, 1400, 2200 and 3000 MPa) and the work-hardening exponent of the Eq. (1) varies between 0.02 and 0.4 (0.02, 0.08, 0.15, 0.22, 0.28, 0.34 and 0.4). The determination of models is then based on 49 materials which have been simulated in order to determine W_e , W_t , $P(h)$ and W_p/W_t changes. The parameters of Eq. (5) corresponding to these 49 materials have been determined (as in the previous paragraph) in order to determine models which depend on the parameters of both Eqs. (1) and (5).

Moreover, in order to make the application of the models to different samples and indenters Young modulus and different indenter radii possible, all the data are determined as functions of σ_y/E^* , n and h/R for Eq. (1) and σ_y/E^* , K/E^* , m and h/R for Eq. (5). In order to have dimensionless data, W_e and W_t are divided by E^*R^3 and $P(h)$ is divided by E^*R^2 .

Fig. 6 shows that the evolution of $-\ln(W_e/E^*R^3)$, W_t/E^*R^3 and $P(h)/E^*R^2$ versus $(-\ln(h/R))$ is well described by an affine function, as for $-\ln(W_p/W_t)$ versus $(-\ln(h/R))$ which is well described by an exponential function. We can also write that

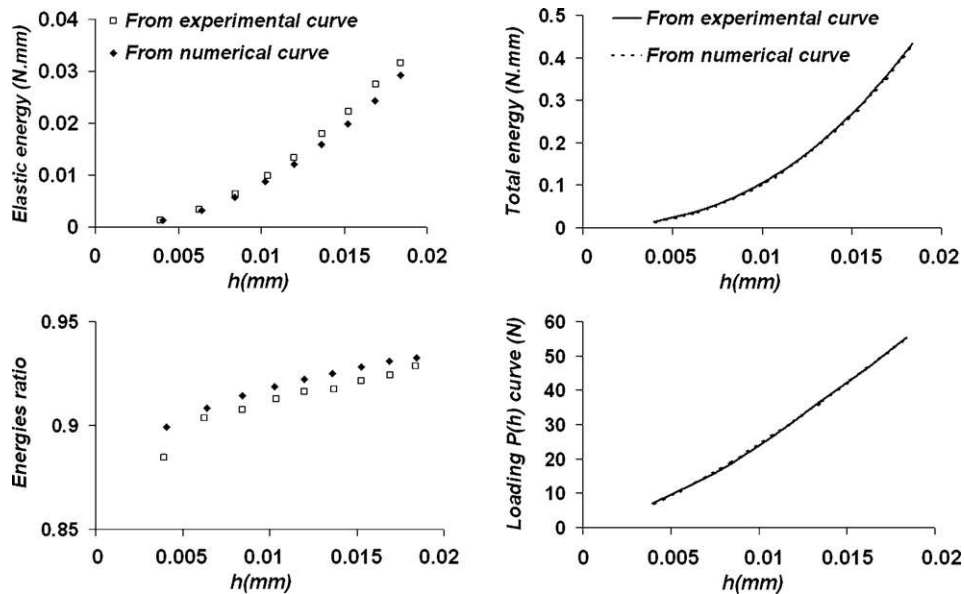


Fig. 10. Comparison between experimental and numerical curves for a C22 steel.

Table 1
Results of the experimental characterization for Eq. (1)

Sample	Exact solution		Minimization on W_e		Minimization on W_t		Minimization on W_p/W_t		Minimization on $P(h)$	
	σ_y (MPa)	n	σ_y (MPa)	n	σ_y (MPa)	n	σ_y (MPa)	n	σ_y (MPa)	n
C22	219	0.16	182	0.21	181	0.16	210	0.21	174	0.19
C100	177	0.24	217	0.25	163	0.22	290	0.25	139	0.27

W_e/E^*R^3 , W_t/E^*R^3 and $P(h)/E^*R^2$ are well described by function j (11) and W_p/W_t by function k (12):

$$j = \left(\frac{h}{R}\right)^A \exp(-B) \quad (11)$$

$$k = \exp\left(-A\left(\frac{h}{R}\right)^{-B}\right) \quad (12)$$

where A and B are quantities depending on σ_y/E^* and n in the case of Eq. (1) and on σ_y/E^* , K/E^* and m in the case of Eq. (5). From the numerical study, a data base of 49 materials leads to 49 W_e , W_t , $P(h)$ and W_p/W_t curves and then to 49 couples (A, B) for each indentation data.

Concerning Hollomon's constitutive Eq. (1), it is possible to represent the evolution of A and B with surfaces which are presented in Fig. B1 (Appendix B). In this figure, functions A and B (z axis) are determined with the software Table Curve 3D. They depend on σ_y/E^* (x axis) and n (y axis). The proposed functions are the ones which give the best correlation coefficient. The coefficients which come in these functions are given in Tables B1 and B2.

Concerning Ludwig's constitutive equation, it is impossible to represent a surface of the evolution of A and B in function of σ_y/E^* , K/E^* and m . These functions have been determined by a minimization with several polynomial functions. If we note $x_1 = \sigma_y/E^*$, $x_2 = K/E^*$ and $x_3 = m$, the best found functions are as follows:

$$A = a + \sum_{i=1}^3 (a_i x_i + b_i x_i^2) + c_1 x_1 x_2 + c_2 x_2 x_3 + c_3 (x_1 x_2)^2 + c_4 (x_2 x_3)^2 \quad (13)$$

$$B = \left(A + \sum_{i=1}^3 (d_i x_i^3) + d_4 x_1 x_3 + d_5 x_1 x_2 x_3 \right)^{-1} \quad (14)$$

The coefficients which come in these functions are given in Tables B3 and B4.

In order to study the accuracy of each model, the comparison has been made between the numerical curves and the prediction

of the model for each indentation data (see Fig. 7 for an example). Concerning the models which depend on Eq. (1) parameters, the average accuracy is 2.5%, 1.0%, 1.6% and 1.5%, respectively for W_e , W_t , W_p/W_t and $P(h)$. For Eq. (5), the average accuracy becomes, respectively 3.7%, 2.6%, 1.1% and 3.4%.

3.4. Study of the uniqueness of the solution

The study of the uniqueness of the solution is based on the minimization between the numerical curves and the proposed models for each indentation data and for the two studied constitutive equations. If we note σ_{num} as a point of a numerical curve, σ_{mod} as a point of the curve obtained from a model and N as the number of points, the minimization is commonly made on the following function:

$$\sum_N (\sigma_{\text{mod}} - \sigma_{\text{num}})^2 \quad (15)$$

Although function (15) gives good results on W_p/W_t , it gives very inaccurate results on W_e , W_t and $P(h)$. Indeed, function (15) does not give the same weight to every point of the curve. Then, we suggest minimizing with the following formula:

$$\sum_N \left(\frac{\sigma_{\text{mod}} - \sigma_{\text{num}}}{\sigma_{\text{num}}} \right)^2 \quad (16)$$

Concerning Hollomon's constitutive equation, formula (16) has been used to inverse the functions (11) and (12) for each indentation data. The results of these inversions, given in Table C1 (Appendix C), show that there is a uniqueness of the solution for each indentation data. We can observe that the lower the work hardening ($n = 0.02$ and 0.08), the lower the precision on the work-hardening exponent n . It can be easily explained with the results of the sensitivity study. Indeed, it has been shown that if the work hardening is low, the sensitivity of the four indentation data to the work hardening is close to 0. If we observe the results of the inversion without considering the lowest values of work-hardening exponent, the average error obtained, respectively on σ_y and n is 3.9% and 4.3% with W_e , 2.9% and 3.4% with W_t , 5.0% and 3.8% with W_p/W_t and 5.8% and 6.5% with $P(h)$. Although the sensitivity study has shown that the most

Table 2
Results of the experimental characterization for Eq. (5)

Sample	Exact solution			Results of minimization		
	σ_y (MPa)	K (MPa)	m	σ_y (MPa)	K (MPa)	m
C22	219	506	0.3175	243	361	0.3214
C100	177	901	0.3789	165	776	0.3618

sensitive data is W_e , it can be observed that the data which gives the best results is W_t . Indeed, this data is less sensitive than W_e , but the model of W_t is the most accurate. Moreover, it has been shown that the sensitivity of W_t and $P(h)$ are quite similar. However, the results of the inversion of W_t model are more accurate (accuracy multiplied by two) than the $P(h)$ ones. Indeed, the model of W_t is more accurate than the $P(h)$ one. It is then shown that both the accuracy of model and the sensitivity explain the accuracy of the inversion.

The energy W_t could be calculated by function (10). It would be then not be necessary to program several loading, unloading and reloading cycles in order to determine the W_t changes. One single loading is sufficient to calculate the W_t changes and then to deduce σ_y and n from inversion. However, the cyclic loading protocol proposed in this paper is very important in the case of Eq. (5).

Indeed, the minimization between models determined for Eq. (5) and numerical curves for each data does not lead to a unique set of σ_y , K and m . Fig. 8 and Table C2 illustrate this fact. Several sets of Eq. (5) parameters lead to the same curve. This shows that one unique indentation data is not sufficient to determine the three parameters of Eq. (5). It is then necessary to minimize (with function (16)) on several indentation data simultaneously. If we consider the four studied data, only two are independent, indeed W_t and $P(h)$ are linked with function (10) and W_e , W_t and W_p/W_t are linked by Eqs. (3) and (4). Although the minimization of both W_t and W_e leads to a unique set of Eq. (5) parameters, for some cases, the results are not very accurate. As an example, for an exact solution $\sigma_y = 2200$ MPa, $K = 6173$ MPa and $m = 0.46$, the minimization with W_e and W_t simultaneously leads to the solution $\sigma_y = 2668$ MPa, $K = 4241$ MPa and $m = 0.44$ and the minimization with W_e , W_t and W_p/W_t simultaneously leads to the solution $\sigma_y = 2340$ MPa, $K = 6343$ MPa and $m = 0.47$. This is the reason why we suggest minimizing, simultaneously, on three indentation data. The model of W_p/W_t is more accurate than the $P(h)$ one and this is the reason why the results presented in Table C3 (middle columns) concern the minimization on W_e , W_t and W_p/W_t simultaneously. It is then shown that the use of three indentation data leads to a unique set of accurate Eq. (5) parameters. However, on the one hand, it can be observed that the lower the work hardening, the lower the accuracy of K . On the other hand very good accuracy is obtained on coefficient m even if the work hardening is low. This can be explained by the form of Eq. (5). In this function, the yield stress σ_y and the work hardening (noted σ_{wh}) are separated. This can be written as

$$\sigma_{wh} = K\varepsilon^m \quad (17)$$

If an error e occurs on the work-hardening evaluation, the new work-hardening function becomes

$$\sigma'_{wh} = (1 + e)K\varepsilon^m = K'\varepsilon^{m'} \quad (18)$$

Function (18) has to be solved for every ε , and the only one solution is $K' = (1 + e)K$ and $m' = m$. In other words, if an error occurs on the work-hardening evaluation, this error will have an effect exclusively on K and not on m . Then, if we calculate the

average error without considering the lowest work hardening values, we obtain 8.2%, 6.5% and 2.1%, respectively for σ_y , K and m .

One can suggest that only the last points of the curves can lead to a unique set of Eq. (5) parameters. This suggestion is true. However, this leads to very inaccurate values of Eq. (5) parameters (see Table C3, last columns).

As a conclusion, although the new cyclic loading protocol is not necessary to determine Eq. (1) parameters, it is necessary to deduce the W_e and W_p/W_t changes and then to deduce accurate values of Eq. (5) parameters.

4. Experimental study

4.1. Presentation

Two steels were selected (a C100 and a C22) because of their microstructure which leads to good homogeneity. For these samples, a tensile test led to the flow stress–strain curve which was fitted by both Eqs. (1) and (5).

We developed an experimental bench which allows the measurement of the $P(h)$ curve with very good reproducibility. The two important parts of this bench are the indenter and the way the displacement is measured.

Concerning the choice of the indenter, the most common spherical indenters are composed of a sphere which is crimped into the body of the indenter. However, the way the sphere is crimped can induce non-negligible deformations between the body of the indenter and the sphere. This is the reason why we chose to use a monobloc indenter. In this indenter, both the body and the spherical part are machined in the same Tungsten carbide piece. However, despite a spherical part being asked for, it was impossible to obtain a perfectly spherical indenter. Fig. 9 shows an image of the indenter realised by electronic scanning microscope from which the true profile of the indenter was measured. It was then shown that there are non-negligible differences between the true profile and a spherical one. However, this indenter can be considered as an axi-symmetric one. In order to compare numerical and experimental curves, the true profile of the indenter was introduced into the FE code as a set of coordinates defining the surface of the indenter.

The displacement was measured by using a capacitive sensor which is fixed near the indenter with an intermediate piece.

Thus our experimental bench allowed us to measure the displacement of the indenter in the sample. However, the needed displacement is the sample surface which is found under the indenter. A previous study [19] proposed a new method to deduce the wanted load–depth curve from the measured one with knowledge of the elastic properties of both the indenter and the sample. This method was based on the determination of the contact radius changes between the indenter and the sample and a modelling of indenter deformations during an indentation test. The contact radius changes were deduced from several loading, unloading and reloading cycles which lead to the determination of the contact stiff-

ness $S(h)$ changes. Moreover, due to the non-spherical indenter, we proposed an equivalent radius function which depends on the contact radius. The new cyclic loading protocol was then necessary to calculate the equivalent radius changes of our indenter and then to deduce the real sample load–depth curve.

4.2. Differences between experimental and numerical curves

In our previous work [19], it has been shown that experimental and numerical loading curves are quite similar. However, we observed non-negligible differences between experimental and numerical unloading curves. At the end of the unloading, the experimental displacement decreased more quickly than the numerical one. Moreover, the reloading cycles sometimes led to the appearance of hysteresis on the $P(h)$ curve. This phenomenon has been observed and studied by several authors. According to Huber and Tsakmakis [20] the hysteresis is the consequence of a kinematic hardening behavior of the tested material. Moreover, they showed that, in the case of pure kinematic behavior, or both isotropic and kinematic behavior, the displacement decreases more quickly than in the case of pure isotropic behavior during the unloading cycle.

Fig. 10 presents the comparison between the studied data deduced from both the experimental and the predicted numerical curve for C22 steel. It is shown that experimental $P(h)$ and W_t changes are well predicted by numerical simulations. However, we can observe large differences between experimental W_e and W_p/W_t changes and the predicted ones.

4.3. Experimental characterization of two steels

Although the differences between experimental and predicted W_e and W_p/W_t changes are non-negligible, we applied function (16) between experiments and models developed for Eq. (1) for each indentation data. The results are presented in Table 1. They confirm that the data which give the most accurate results is the W_t changes (average accuracy 13% on σ_y and 4% on n). The inversion of the $P(h)$ curve gives less accurate results than W_t , which can be explained by the accuracy of the corresponding model. Concerning the indentation data which are affected by the unloading, the accuracy of results obtained from the inversion of W_e is near to that obtained for $P(h)$ inversion. This can be explained by the high sensitivity of W_e which compensates the differences between experimental and numerical unloading. Lastly, W_p/W_t gives the least accurate results.

Concerning the determination of the parameters of Eq. (5), the minimization with W_e , W_t and W_p/W_t simultaneously or W_e , W_t and $P(h)$ simultaneously gives very inaccurate results. However, the minimization on W_t changes leads to a unique set of parameters. Although it has been shown in the numerical study that there is no uniqueness if the minimization is made on only one indentation data, we observed uniqueness in this experimental study. This can be explained by the use of a non-spherical indenter with an equivalent radius function. Thus, an

indentation test with this kind of indenter can be assimilated to several indentations with different indenter radii. The results of inversion of W_t changes for Eq. (5) are given in Table 2. The average accuracy is 9% on σ_y , 21% on K and 3% on m .

As a conclusion, although some differences occurred between experimental and numerical results, the inversion of models proposed in the numerical study led to an evaluation of the parameters which are in Eqs. (1) and (5). These results also showed that methods based on a “reverse” analysis are limited in accuracy, the more the number of mechanical parameters the less the accuracy of the characterization. This kind of method can be used in order to have an evaluation of the mechanical behavior in a first-order approximation. However, in order to have a more accurate characterization, it will be necessary to use other kinds of methods such as the “inverse” analysis.

5. Conclusion

A new kind of indentation protocol is proposed in this paper. It is composed of several loading, unloading and reloading cycles which allow the determination of the indentation data changes. In this study, four indentation data are studied: the elastic and total energies W_e and W_t , the plastic to total energy ratio W_p/W_t and the loading $P(h)$ curve. From a numerical study, models describing these data changes have been determined for two constitutive equations with isotropic hardening. These models have allowed us to study the uniqueness of the solution for the two studied constitutive equations. For the first equation with two plasticity parameters, only one indentation data is sufficient to determine the mechanical properties with good accuracy. Moreover, from the numerical results, the best data is the total energy W_t which can be deduced without cyclic loading. However, for the second constitutive equation with three plasticity parameters, it has been shown that several loading, unloading and reloading cycles are necessary to determine accurate values of the mechanical parameters. The numerical study has also shown that both the sensitivity and the accuracy of models explain the accuracy of the results.

In a previous paper, we have shown that the proposed cyclic loading protocol is necessary to deduce the real load–depth curve from the measured one. It is then shown that some differences occur between experimental and numerical unloading curves. These differences justify the low accuracy obtained by inversion of data which depends on the unloading. However, inversion of the total energy which is not sensitive to these problems leads to an evaluation of the parameters of the two studied constitutive equations. In this case, the uniqueness with the second constitutive equation can be explained by the use of an indenter which can be assimilated to several indenters with different radii which are calculated using the new cyclic loading protocol.

It has thus been shown in this paper that in order to evaluate more than two mechanical parameters, it is necessary to increase the experimental data field either by using several indentation data changes or several indenter radii.

Lastly, this paper shows that methods based on a “reverse” analysis lead to a more or less accurate determination of the mechanical properties. They can, however, give an evaluation of the material’s behavior in a first-order approximation and then can be used in order to have a comparison between several materials. The study of other kinds of methods like “inverse” analysis is one of our perspectives in order to increase the accuracy of the characterization.

Acknowledgment

This research was sponsored by the Brittany Region.

Appendix A. Sensitivity study

Fig. A1.

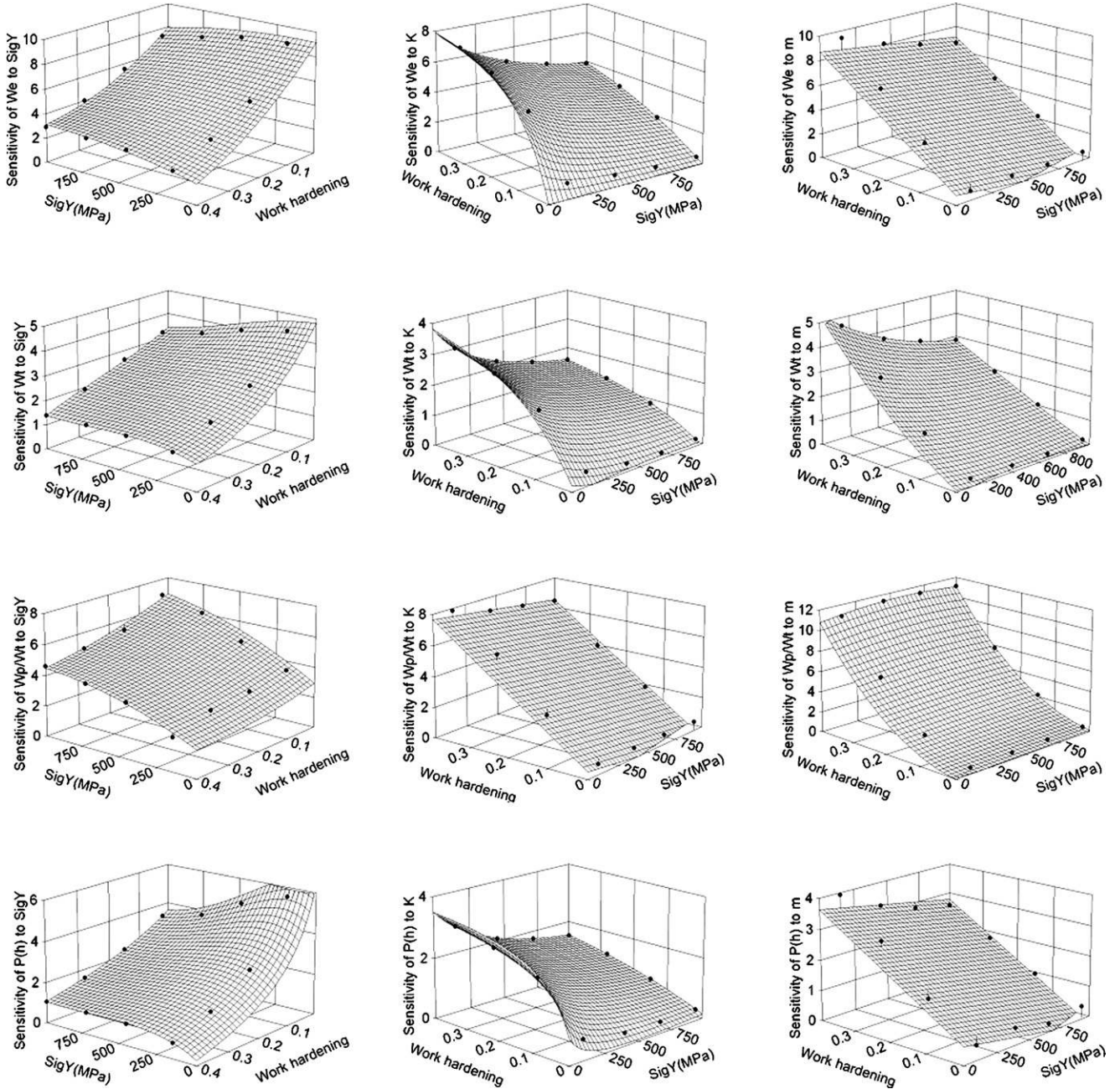


Fig. A1. Sensitivity changes for each studied indentation data.

Appendix B. Determination of the models

Fig. B1.

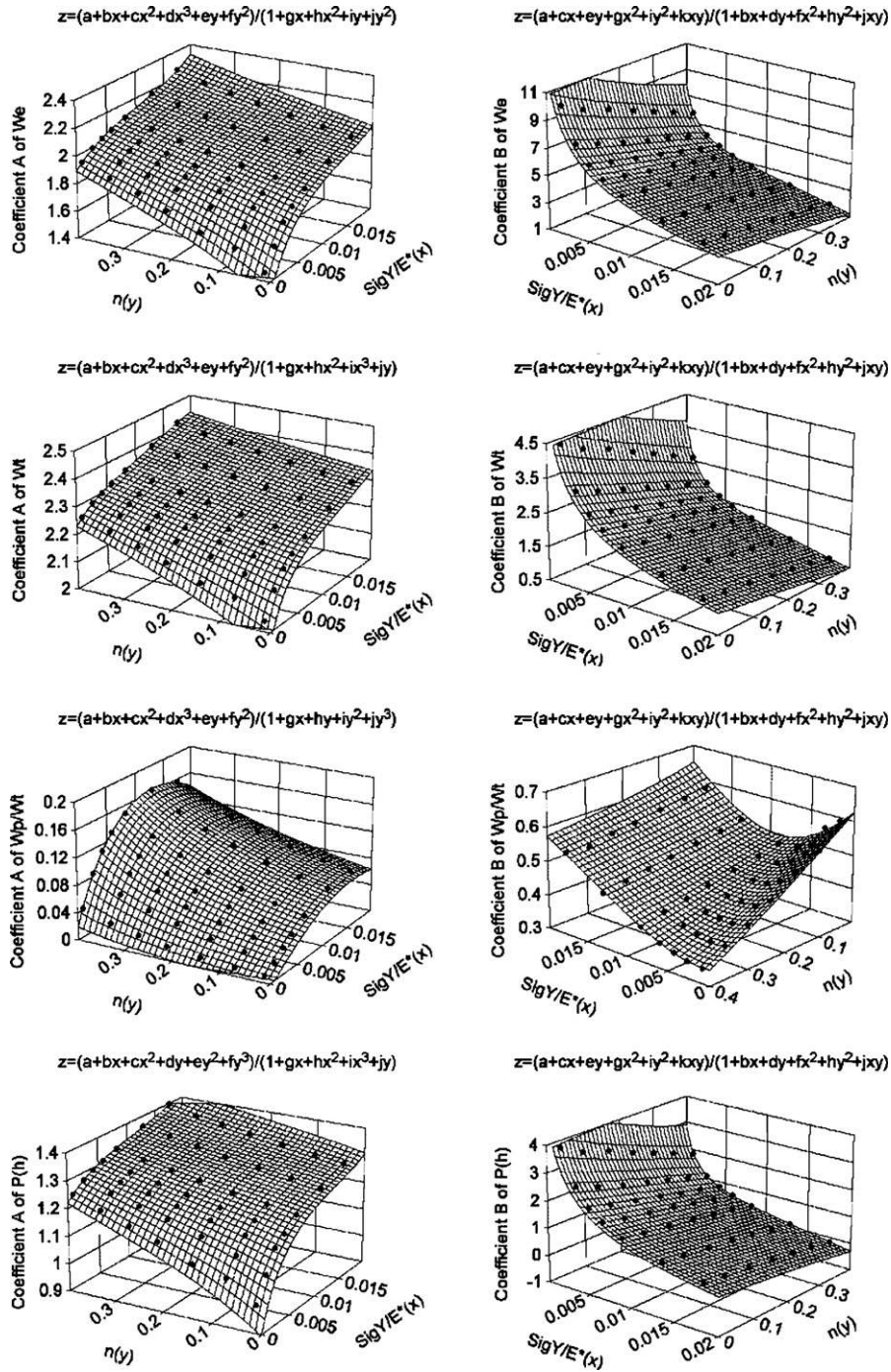


Fig. B1. Functions A and B which come in Eqs. (11) and (12).

Tables B1–B4.

Table B1

Coefficients which come in function A for Eqs. (11) and (12)

Data	a	b	c	d	e	f	g	h	i	j
W_e	1.2337	368.7702	-16397.8780	44854.0970	5.7106	-2.6740	150.2944	-70.235686	2.4492	-2.0914
W_t	1.9315	526.6240	-45734.4050	1096080.2000	5.1262	0.7832	212.8758	-19375.6920	468759.1300	2.1066
W_p/W_t	-0.0075	8.2528	40.1633	-9737.7621	0.0533	-0.0566	26.1103	-2.0304	0.0756	0.8071
$P(h)$	0.8946	227.6553	-10699.6670	3.6171	0.0717	1.3472	143.5716	-6922.8572	-26221.0330	2.5028

Table B2

Coefficients which come in function B for Eqs. (11) and (12)

Data	a	b	c	d	e	f	g	h	i	j	k
W_e	12.8151	367.3677	844.7441	-0.7832	-27.8083	-4794.3394	-27014.0050	-1.8007	9.0035	-253.6345	-578.8095
W_t	5.7879	405.2397	392.1503	-0.6645	-11.3579	-4573.9157	-14009.3360	-1.8652	2.2474	-215.9234	-192.3363
W_p/W_t	0.6262	-23.8830	-41.0306	0.4967	-0.4412	2001.3517	2631.3604	0.5303	-0.0343	187.6590	137.6183
$P(h)$	5.3303	309.8288	22.8952	-0.7235	-12.9210	-4693.6406	-7502.3214	-1.9085	6.2890	-303.3440	18.4632

Table B3

Coefficients of function f_1 (Eq. (13))

Data	a	a_1	a_2	a_3	b_1	b_2	b_3	c_1	c_2	c_3	c_4
W_e	0.4799	9.5799	-2.5683	5.8946	-2.8629	1.0695	-6.1122	-6.9739	9.5389	0.9933	-0.0315
W_t	1.5875	6.5688	-1.2094	2.7659	-3.3348	-2.6223	-2.9957	-7.8405	5.1887	0.9918	-1.2836
W_p/W_t	0.0042	8.5243	4.2597	-0.0769	-256.8118	-8.2117	0.1465	-71.0339	-4.6614	0.9360	35.7140
$P(h)$	0.5729	6.7193	-1.3417	2.8247	-3.3598	-2.5429	-3.0331	-7.9480	5.2952	0.9915	-1.2600

Table B4

Coefficients of function f_2 (Eq. (14))

Data	a	a_1	a_2	a_3	b_1	b_2	b_3	c_1	c_2	c_3	c_4	d_1	d_2	d_3	d_4	d_5
W_e	-0.0592	29.4613	18.7065	1.4148	185.1068	8.0161	-4.5846	-621.6012	-33.8156	68.1669	-275843	14.2524	28.0201	5.0787	-53.8962	1563.7558
W_t	-0.1473	62.0351	34.2116	3.2741	219.9531	24.2602	-10.5230	-473.9512	-63.7603	68.4722	-13.9860	16.2688	40.0677	11.8180	-89.7697	1641.1261
W_p/W_t	0.4784	67.6387	10.8059	6.2035	188.2657	-7.8024	-3.2472	-517.1911	-27.8351	68.4045	-25.3187	15.4058	32.9577	4.5077	-321.2930	1619.2977
$P(h)$	0.4072	56.1993	113.1517	7.5934	117.8745	808.9538	-31.7259	-78.3279	-303.3418	68.5109	211.3025	13.7692	132.8986	44.6494	45.6690	1828.5915

Appendix C. Study of the uniqueness of the solution

Tables C1–C3

Table C1

Results of inversion of models for each indentation data

Exact solution		Minimization on W_e		Minimization on W_t		Minimization on W_p/W_t		Minimization on $P(h)$	
σ_y (MPa)	n	σ_y (MPa)	n	σ_y (MPa)	n	σ_y (MPa)	n	σ_y (MPa)	n
150	0.02	144	0.02	153	0.01	204	0.03	230	0.00
150	0.08	137	0.10	124	0.11	148	0.11	161	0.10
150	0.15	172	0.13	150	0.14	148	0.16	165	0.13
150	0.22	159	0.21	150	0.22	134	0.23	132	0.22
150	0.28	147	0.28	154	0.28	131	0.29	131	0.28
150	0.34	136	0.34	157	0.34	136	0.34	139	0.34
150	0.4	117	0.41	149	0.4	127	0.41	147	0.4
450	0.02	453	0.00	487	0.00	433	0.00	446	0.00
450	0.08	471	0.07	461	0.08	394	0.10	411	0.09
450	0.15	451	0.15	450	0.15	393	0.17	392	0.18
450	0.22	459	0.23	455	0.22	410	0.24	404	0.24

Table C1 (Continued).

Exact solution		Minimization on W_e		Minimization en W_t		Minimization on W_p/W_t		Minimization on $P(h)$	
σ_y (MPa)	n	σ_y (MPa)	n	σ_y (MPa)	n	σ_y (MPa)	n	σ_y (MPa)	n
450	0.28	455	0.28	456	0.28	439	0.29	427	0.29
450	0.34	455	0.34	446	0.34	458	0.34	449	0.35
450	0.4	454	0.40	408	0.41	439	0.4	451	0.40
720	0.02	673	0.04	728	0.02	561	0.08	596	0.08
720	0.08	688	0.10	707	0.09	615	0.12	639	0.11
720	0.15	693	0.17	707	0.16	661	0.17	667	0.17
720	0.22	712	0.23	714	0.23	722	0.22	708	0.23
720	0.28	720	0.28	721	0.28	745	0.28	724	0.28
720	0.34	734	0.34	713	0.34	759	0.33	755	0.33
720	0.4	738	0.40	648	0.41	736	0.4	755	0.39
1000	0.02	947	0.04	994	0.02	877	0.06	932	0.04
1000	0.08	935	0.10	978	0.09	916	0.11	952	0.10
1000	0.15	957	0.17	978	0.16	1004	0.16	1020	0.15
1000	0.22	985	0.22	996	0.22	1063	0.21	1056	0.20
1000	0.28	1000	0.28	1017	0.27	1050	0.28	1074	0.26
1000	0.34	1023	0.33	1023	0.33	1047	0.34	1079	0.33
1000	0.4	1034	0.39	956	0.40	1007	0.40	1057	0.39
1400	0.02	1410	0.02	1387	0.02	1370	0.03	1395	0.02
1400	0.08	1386	0.08	1367	0.09	1437	0.08	1462	0.07
1400	0.15	1400	0.15	1382	0.15	1492	0.14	1519	0.12
1400	0.22	1416	0.21	1419	0.21	1487	0.21	1534	0.19
1400	0.28	1425	0.27	1454	0.27	1451	0.28	1505	0.26
1400	0.34	1442	0.33	1474	0.33	1427	0.34	1494	0.32
1400	0.4	1450	0.39	1432	0.40	1382	0.40	1440	0.39
2200	0.02	2350	0.00	2076	0.05	2279	0.02	2205	0.02
2200	0.08	2254	0.07	2092	0.10	2269	0.08	2240	0.07
2200	0.15	2192	0.15	2133	0.16	2246	0.14	2232	0.14
2200	0.22	2155	0.23	2206	0.22	2190	0.22	2155	0.23
2200	0.28	2132	0.29	2295	0.26	2136	0.28	2086	0.30
2200	0.34	2101	0.36	2375	0.31	2095	0.34	1999	0.37
2200	0.4	2050	0.43	2448	0.36	2059	0.40	1806	0.45
3000	0.02	2940	0.04	2891	0.06	2953	0.03	2851	0.05
3000	0.08	2836	0.11	3018	0.08	2950	0.09	3093	0.06
3000	0.15	2786	0.19	2938	0.17	2932	0.16	2844	0.18
3000	0.22	2775	0.25	3012	0.22	2891	0.23	2904	0.24
3000	0.28	3016	0.27	2994	0.28	2882	0.29	2978	0.2S
3000	0.34	2927	0.34	2990	0.33	2813	0.35	2972	0.33
3000	0.4	2809	0.44	2695	0.45	3214	0.45	2954	0.41

Table C2

Several sets of parameters can lead to the same curve

Exact solution		Minimization on W_e		Minimization on W_t		Minimization on W_p/W_t		Minimization on $P(h)$	
		1	2	1	2	1	2	1	2
σ_y (MPa)	450	1253	1426	1180	1058	920	1398	900	200
K (MPa)	2159	391	0	0	356	998	0	0	3864
m	0.39	0.36	0.36	0.35	0.36	0.39	0.41	0.34	0.49

Table C3

Results of the minimization with W_e , W_t and W_p/W_t for Eq. (5)

Exact solution			Minimization on data changes			Minimization on the last points		
σ_y (MPa)	K (MPa)	m	σ_y (MPa)	K (MPa)	m	σ_y (MPa)	K (MPa)	m
150	25	0.2031	156	14	0.2064	3	368	0.3381
150	123	0.2336	143	143	0.2455	61	458	0.3331
150	307	0.2728	148	289	0.2652	77	593	0.3359
150	609	0.3158	171	553	0.3048	155	621	0.3169
150	1,020	0.3554	184	935	0.3431	190	814	0.3257
150	1,653	0.3973	182	1,551	0.3886	80	1993	0.4241
150	2,628	0.4410	139	2,566	0.4390	135	2560	0.4383
450	63	0.2487	445	75	0.2522	453	32	0.2481
450	304	0.2772	359	393	0.2658	485	144	0.2588
450	720	0.3132	393	724	0.3005	526	214	0.2574
450	1,355	0.3520	444	1,187	0.3354	563	360	0.2661
450	2,159	0.3873	505	1,727	0.3662	540	1294	0.3382
450	3,317	0.4244	552	2,680	0.4063	645	1293	0.3324
450	4,990	0.4628	414	4,828	0.4579	534	4076	0.4409
720	93	0.2737	646	195	0.2753	673	100	0.2680
720	444	0.3011	647	447	0.2905	702	235	0.2760
720	1,031	0.3353	622	1,086	0.3257	741	430	0.2873
720	1,897	0.3719	687	1,862	0.3665	791	807	0.3105
720	2,961	0.4051	770	2,834	0.4066	785	2440	0.3903
720	4,451	0.4397	713	4,545	0.4465	730	4362	0.4424
720	6,549	0.4755	778	5,529	0.4608	739	4503	0.4521
1000	123	0.2936	802	481	0.2999	858	264	0.2886
1000	577	0.3200	818	1,093	0.3352	884	533	0.3036
1000	1,322	0.3529	887	1,497	0.3519	903	1214	0.3379
1000	2,394	0.3878	1084	1,910	0.3744	868	3534	0.4262
1000	3,685	0.4193	1150	3,617	0.4283	843	4863	0.4500
1000	5,459	0.4520	1039	5,655	0.4612	879	5872	0.4601
1000	7,910	0.4858	1013	7,235	0.4808	887	6882	0.4638
1400	162	0.3164	1404	304	0.3309	1092	1056	0.3413
1400	753	0.3416	1381	973	0.3523	1100	1858	0.3712
1400	1,699	0.3728	1422	1,760	0.3770	1114	3146	0.4100
1400	3,030	0.4059	1488	2,938	0.4089	1062	5299	0.4548
1400	4,600	0.4356	1572	4,416	0.4422	1001	7167	0.4755
1400	6,716	0.4663	1674	6,535	0.4796	931	8960	0.4843
1400	9,587	0.4979	1449	9,598	0.4990	3415	174	0.4010
2200	233	0.3510	2405	214	0.3689	1488	3502	0.4173
2200	1,069	0.3744	2271	1,084	0.3790	2791	0	0.3823
2200	2,368	0.4030	2184	2,404	0.4010	2911	363	0.3885
2200	4,141	0.4335	2210	4,210	0.4343	2896	1185	0.3962
2200	6,173	0.4605	2340	6,344	0.4717	2865	2258	0.4084
2200	8,847	0.4883	2391	9,481	0.5114	2823	4443	0.4399
2200	12,386	0.5168	2185	12,313	0.5134	3026	4718	0.4372
3000	298	0.3775	2985	572	0.3833	2329	3226	0.4156
3000	1,353	0.3997	2868	1,463	0.3914	2419	3918	0.4270
3000	2,962	0.4270	2764	3,046	0.4123	2615	4366	0.4334
3000	5,111	0.4549	2788	5,446	0.4485	2791	4643	0.4345
3000	7,326	0.4720	2950	8,176	0.4870	2971	4900	0.4328
3000	10,674	0.5146	2832	11,619	0.5121	3111	5173	0.4322
3000	14,074	0.5039	2810	15,005	0.5084	3359	5787	0.4307

References

- [1] H. Hertz, *Z. Reine Angew. Math.* 92 (1882) 156–171.
- [2] I.N. Sneddon, *Int. J. Eng. Sci.* (1965) 3.
- [3] S.I. Bulychev, V.P. Alekhin, *Zavod Lab.* (1975) 41.
- [4] M.Kh. Shorshorov, S.I. Bulychev, V.P. Alekhin, *Sov. Phys. Dokl.* (1982) 26.
- [5] A.P. Ternovskii, V.P. Alekhin, M.Kh. Shorshorov, M.M. Khurshchov, V.N. Skvortsov, *Zavod Lab.* 39 (1973) 1973.
- [6] M.F. Doerner, W.D. Nix, *J. Mater. Res.* (1986) 1.
- [7] J.L. Loubet, J.M. Georges, G. Meille, Vickers in dentation curves of elastoplastic materials, in: *Microindentation Techniques in Materials Science and Engineering*, ASTM STP 889, 1986.
- [8] W.C. Oliver, G.M. Pharr, *J. Mater. Res.* 7 (6) (1992) 1564–1583.
- [9] J.C. Hay, P.J. Wolff, *J. Mater. Res.* 16 (5) (2001) 1280–1286.
- [10] T. Nakamura, T. Wang, S. Sampath, *Acta Mater.* 48 (2000) (2000) 4293–4306.
- [11] Bolzon, G. Maier, M. Panico, *Int. J. Sol. Struct.* 41 (2004) (2004) 2957–2975.
- [12] D. Tabor, *Hardness of Metals*, Clarendon Press, Oxford, 1908.

- [13] M. Dao, N. Chollacoop, K.J. Van Vliet, T.A. Venkatesh, S. Suresh, *Acta Mater.* 49 (2001) 3899–3918.
- [14] N. Chollacoop, M. Dao, S. Suresh, *Acta Mater.* 51 (2003) 3713–3729.
- [15] J.L. Bucaille, S. Strauss, E. Felder, J. Michler, *Acta Mater.* 51 (6) (2003) 1669–1678.
- [16] Y.T. Cheng, C.M. Cheng, *Mater. Sci. Eng. R* 44 (2004) 91–149.
- [17] Y.P. Cao, J. Lu, *Acta Mater.* 52 (2004) 4023–4032.
- [18] M. Beghini, L. Bertini, V. Fontanari, *Int. J. Sol. Struct.* (2005).
- [19] J.-M. Collin, G. Mauvoisin, R. El Abdi, *Mech. Mater.* 40 (2008) 401–406.
- [20] N. Huber, Ch. Tsakmakis, *Mech. Mater.* 27 (1998) (1997) 241–248.